Check for updates

Ultrafast dynamics in co-sensitized photocatalysts under visible and NIR light irradiation

Jayita Patwari,[a] Arka Chatterjee,[a] Samim Sardar, [ID][a] Peter Lemmens[bc] and Samir Kumar Pal [ID] *[a]

Co-sensitization to achieve a broad absorption window is a widely accepted technique in light harvesting nanohybrid synthesis. Protoporphyrin (PPIX) and squaraine (SQ2) are two organic sensitizers absorbing in the visible and NIR wavelength regions of the solar spectrum, respectively. In the present study, we have sensitized zinc oxide (ZnO) nanoparticles using PPIX and SQ2 simultaneously for their potential use in broad-band solar light harvesting in photocatalysis. Förster resonance energy transfer (FRET) from PPIX to SQ2 in close proximity to the ZnO surface has been found to enhance visible light photocatalysis. In order to confirm the effect of intermolecular FRET in photocatalysis, the excited state lifetime of the energy donor dye PPIX has been modulated by inserting d^{10} (Zn^{II}) and d^7 (Co^{II}) metal ions in the central position of the dye (PP(Zn) and PP(Co)). In the case of PP(Co)–SQ2, extensive photo-induced ligand to metal charge transfer counteracts the FRET efficiency while efficient FRET has been observed for the PP(Zn)–SQ2 pair. This observation has been justified by the comparison of the visible light photocatalysis of the respective nanohybrids with several control studies. We have also investigated the NIR photocatalysis of the co-sensitized nanohybrids which reveals that reduced aggregation of SQ2 due to co-sensitization of PPIX increases the NIR photocatalysis. However, core-metalation of PPIX reduces the NIR photocatalytic efficacy, most probably due to excited state charge transfer from SQ2 to the metal centre of PP(Co)/PP(Zn) through the conduction band of the host ZnO nanoparticles.

1. Introduction

The efficient conversion of solar light into chemical and electrical energy has been attracting expanding scientific and technological interest in order to address the scarcity of energy resources and enormous environmental pollution.[1–4] Photocatalysis is a technique used for the degradation of toxic organic pollutants by formation of oxidizing free radicals, utilizing renewable solar energy.[5,6] Thus, development of novel materials with efficient photocatalytic activity, enough stability and a well-matched absorption with the solar spectrum has been recognized as an essential step to combat environmental pollution through solar energy conversion.[7–10] Sensitization of wide bandgap semiconductor photocatalysts such as TiO_2 and ZnO with dyes to increase the photo response in the visible region is well documented in the literature but materials harvesting in the NIR region which constitutes 49% of the

entire solar spectrum are still less explored.[11,12] The use of organic dyes is favorable as a sensitizer when compared to metal-based dyes as they are relatively cheap, less toxic and possess a higher molar absorption coefficient.[13,14] However, it is very difficult to emulate the solar spectra with a single organic dye sensitizer because of the characteristic narrow absorption band of most of the organic sensitizers.[15] To resolve this problem, co-sensitization of two dyes has been a well-known technique in the case of dye-sensitized solar cells (DSSCs).[16,17] However, co-sensitization using more than two sensitizers is less studied in the case of photocatalysis.[18,19] Co-sensitization may bring some additional difficulties to the system because of the unwanted synergistic carrier mechanism and the interactions occurring between the sensitizers.[20–22] Hence, in order to achieve enhanced catalytic activity through co-sensitization, the choice of the sensitizers is supposed to be enough justified and the elucidation of photo-physical properties and ultrafast carrier dynamics of the sensitizers is indispensable.

In our earlier work, protoporphyrin IX (PPIX) sensitized ZnO has been proved to be a good visible light-induced photocatalyst due to the appropriate alignment of the conduction band of ZnO and the highest occupied molecular orbital (HOMO) of the dye.[23] However, the main limitation of the porphyrin sensitized photocatalysts has been found to be poor

[a] *Department of Chemical, Biological and Macromolecular Sciences, S. N. Bose National Centre for Basic Sciences, Block JD, Sector III, Salt Lake, Kolkata 700 106, India. E-mail: skpal@bose.res.in*

[b] *Institute for Condensed Matter Physics, TU Braunschweig, Mendelssohnstraße 3, 38106 Braunschweig, Germany*

[c] *Laboratory for Emerging Nanometrology, TU Braunschweig, Braunschweig, Germany*

10418 | *Phys. Chem. Chem. Phys.*, 2018, **20**, 10418–10429

This journal is © the Owner Societies 2018

absorbance in the red and near infrared (NIR) wavelength range. Recently, different squaraine dyes have stimulated a lot of attention as a NIR absorbing sensitizer in the field of DSSCs,[24–26] organic solar cells[27,28] and photocatalysis[29,30] although they have a much reported self-aggregation problem.[31,32] In a recent publication, we have successfully avoided the problem of sensitizer squaraine (SQ2) aggregation using PPIX as a co-sensitizer. Additionally, the increased absorption window due to co-sensitization and dipolar coupling between the sensitizer–co-sensitizer couple has been found to improve the efficiency in DSSCs.[33] It has to be noted that the PPIX dye from natural resources has a metal ion at the central position of the dye. The impact of different metal ions in the porphyrin cavity on ultrafast photoinduced dynamics has been widely reported[34,35] and their implications in photocatalysis are also studied in our previous publication.[36] However, the role of different metal ions in porphyrin to determine the dipole–dipole coupling (FRET) with other organic dyes on a semiconductor surface and its implication in visible and NIR light harvesting is sparsely reported in the literature.

In the present study, we have co-sensitized ZnO nanoparticles with SQ2 (NIR absorbing dye) and PPIX (visible light absorbing dye). The Förster resonance energy transfer (FRET) between the acceptor SQ2 and the donor PPIX has been observed from time resolved fluorescence measurements and it has been found to play a beneficial role in providing enhanced catalytic activity apart from increasing the absorption window. For comparative studies, we have synthesized co-sensitized nanohybrids by impregnating a PPIX moiety with different d-block metal ions (Zn and Co), which is expected to modulate the excited state lifetime of the energy donor at the surfaces of the host nanoparticles. Picosecond resolved fluorescence spectroscopy has been used to investigate the changes in FRET efficiency of PPIX upon metalation in the presence of the acceptor dye SQ2. The effect of FRET between the two co-sensitizers has been correlated with the modulation of the visible light induced catalytic activity of their respective co-sensitized nanohybrid. We have also investigated NIR catalysis upon metalation of PPIX in the synthesized nanohybrid. In the case of NIR catalysis, the suppression of aggregation of the SQ2 molecules due to co-sensitization is observed to enhance the catalytic activity of the PPIX–SQ2 co-sensitized nanohybrid. However, metalation of the PPIX co-sensitizer has reduced the efficacy of the NIR catalysis of the SQ2-sensitized nanohybrid. We have provided a mechanistic explanation for catalytic activity modulation of different co-sensitized nanohybrids under visible and NIR light irradiation by unraveling ultrafast excited state dynamic events.

2. Experimental section

2.1. Reagents

All the chemicals used in this study were of analytical grade and used without any further purification. ZnO nanoparticles (~30 nm), protoporphyrin IX [PPIX], cobalt(II) chloride

hexahydrate [$CoCl_2\cdot 6H_2O$], aluminium oxide nanopowder (<50 nm), and zinc(II) nitrate hexahydrate [$Zn(NO_3)_2\cdot 6H_2O$] were purchased from Sigma-Aldrich. Squaraine (SQ2) from Solaronix, dimethyl sulfoxide (DMSO) from Merck, and ultrapure water of Millipore System (18.2 MΩ cm) were used in the present study.

2.2. Preparation of dye solutions

0.3 mM PPIX and 0.3 mM SQ2 solutions were prepared separately under constant stirring for 1 h, using dimethyl sulfoxide (DMSO) as a solvent. DMSO was used as a solvent because both the dyes have good solubility in DMSO and it is an accepted biologically relevant solvent.[37] These two dye solutions were mixed at different molar ratios such as (SQ2 : PPIX) 8 : 2, 6 : 4, 4 : 6, and 2 : 8 and the dye cocktails were named accordingly as S8P2, S6P4, S4P6, and S2P8. For the preparation of the cobalt(II) ion metalated porphyrin [PP(Co)] solution an excess amount of (1 : 10 molar ratio) cobalt(II) chloride hexahydrate was added to 0.3 mM PP dye solution in DMSO and the mixture was allowed for overnight stirring. For the preparation of PP(Zn), core metalation was done using the same procedure as cobalt(II) using the salt zinc(II) nitrate hexahydrate. SQ2 and PP(Co) were mixed at a molar ratio of 8 : 2 for the preparation of another co-sensitizer solution and the SQ2 and PP (Zn) mixture was also prepared using the same molar ratio.

2.3. Synthesis of the co-sensitized nanohybrid

ZnO NPs were sensitized with each of the above-mentioned individual dyes and their respective dye cocktails by adding 20 mg of ZnO NPs to 10 mL of each dye solution with continuous stirring for 12 h, at room temperature. After sensitization, the solutions were centrifuged for some time and the clear supernatants containing the unbound dyes were separated out. Then, the sensitized nanohybrids were washed with DMSO for several times to remove the possible unbound or loosely bound dyes from the surface of the nanoparticles. The nanohybrids were then dried by heating on a water bath and stored in the dark.

2.4. Methods of characterization

All the absorption spectra were recorded on a Shimadzu UV-2600 spectrophotometer. The steady-state emission and excitation spectra were recorded on a Jobin Yvon Fluorolog fluorimeter. The picosecond time resolved fluorescence transients were measured using a time correlated single photon counting (TCSPC) setup from Edinburgh Instruments. Picosecond pulsed lasers of Pico-quant (633 nm and 409 nm wavelengths) were used as excitation sources in this study. The instrument response function (IRF) was measured to be 80 ps. The experimental setup and fitting parameters are discussed in detail in the earlier publications from our group.[38] The peak counts of the TCSPC measurements were maintained at 2000 and at this count, a reasonably good signal to noise ratio was achieved. The FRET efficiency between the acceptor (SQ2) and different donors (PPIX, PP(Zn)) was studied using the reported methodology.[39] The equations for calculating the Förster distance (R_0 in Å) and energy transfer efficiency between the donor and the acceptor

This journal is © the Owner Societies 2018

Phys. Chem. Chem. Phys., 2018, **20**, 10418–10429 | 10419

were reported earlier.[40] The Förster resonance energy transfer (FRET) has been studied between the donor PPIX or PP(Zn) and the acceptor (SQ2) by calculating the Förster distance (R_0 in Å)

$$R_0 = 0.211 \times \left[\kappa^2 n^{-4} Q_D J\right]^{\frac{1}{6}} \qquad (1)$$

where κ^2 is the factor describing the relative orientation in space of the transition dipoles of the donor and the acceptor and the magnitude is assumed to be 2/3. The refractive index (n) of the medium is calculated to be 1.479. The quantum yields of the donors PPIX and PP(Zn) were calculated to be 0.06 and 0.01, respectively. J, the overlap integral, which expresses the degree of spectral overlap between the donor emission and the acceptor absorption, is given by,

$$J(\lambda) = \frac{\int_0^\infty F_D(\lambda)\varepsilon_A(\lambda)\lambda^4 d\lambda}{\int_0^\infty F_D(\lambda)d\lambda} \qquad (2)$$

where $F_D(\lambda)$ is the fluorescence intensity of the donor in the wavelength range of λ to $\lambda + d\lambda$ and is dimensionless; $\varepsilon_A(\lambda)$ is the extinction coefficient (in $M^{-1}\ cm^{-1}$) of the acceptor at λ. If λ is in nm, then J is in units of $M^{-1}\ cm^{-1}\ nm^4$. The donor–acceptor distance (r_{DA}) can be easily calculated using the formula,

$$r_{DA}{}^6 = \frac{\left[R_0{}^6(1-E)\right]}{E} \qquad (3)$$

Here E is the efficiency of energy transfer. The transfer efficiency is measured using the relative fluorescence lifetime of the donor, in the absence (τ_D) and presence (τ_{DA}) of the acceptor.

$$E = 1 - \frac{\tau_{DA}}{\tau_D} \qquad (4)$$

From the average lifetime calculation for PPIX_SQ2 and PP(Zn)_SQ2, we obtain the effective distance between the donor and the acceptor (r_{DA}), using the above equations. The molar extinction co-efficient of the acceptor SQ2 was considered to be 319 000 $M^{-1}\ cm^{-1}$ as per reported literature.[41] The reflecting mode absorption spectra of the nanohybrids were collected using a StellarNet™ spectrograph in the diffuse reflectance technique.

2.5. Methods for photocatalysis test

The photocatalytic activity of the nanohybrids under visible light illumination was examined for photo-decomposition of acridine orange (AO), a model pollutant having a nitrogen containing heterocyclic structure in aqueous solution. The photodegradation of AO (initial concentration $C_0 = 0.5 \times 10^{-4}$ M) was carried out in a 1 cm optical path quartz cell containing 3 mL of solution having 1 g L^{-1} concentration of each nanohybrid. The suspension was irradiated under visible light using a mercury lamp of 7800 Lux, with a 395 nm high pass filter and appropriate amounts of aliquots were taken out at certain time intervals. The percentage degradation (%DE) of AO in 1 h was calculated using eqn (5):

$$\% \text{ DE} = \frac{I_0 - I}{I_0} \times 100 \qquad (5)$$

where I_0 is the initial absorption intensity of AO at $\lambda_{max} = 491$ nm and I is the absorption intensity after 1 h visible light irradiation.

On the other hand, NIR catalysis was performed using a tungsten–halogen lamp with a 650 nm high pass filter. The intensity of this particular lamp was measured to be 31200 Lux.

3. Results and discussion

Un-metalated protoporphyrin (PPIX) and squaraine (SQ2) are two commercially available dyes which have been chosen in this study as co-sensitizers. The other two dyes, cobalt(II) metalated protoporphyrin (PP(Co)) and zinc(II) metalated protoporphyrin (PP(Zn)), are synthesized by core metalation of the protoporphyrin moiety following the procedure mentioned in the Experimental section. Although the acidic pK_a value of the protonated imino nitrogens facilitates the reaction of core metalation, the process is highly selective upon the choice of metal ions. The absorption spectrum of PPIX (Fig. 1a) in DMSO solvent shows the strongest intensity peak at 407 nm, which is due to the Soret band transition (B band), and the other four lower intensity Q band peaks appear at 507 nm, 543 nm, 575 nm and 630 nm. Both the B and the Q bands arise from π–π^* transitions. The four Q bands are the X and Y components of the two vibronic transitions between $S_1 \leftarrow S_0$ electronic levels. The changes in the absorption spectra of PP(Zn) (Fig. 1b) and PP(Co) (Fig. 1c) when compared to that of PPIX can be considered as evidence of metalation in the "pocket" of the porphyrin ligand. The red shifted Soret band and two vanished Q bands are typical signatures of the metal ion incorporation. For PP(Zn) the Soret band maxima appears at 421 nm and the two prominent Q bands appear at 547 nm and 584 nm. In the case of PP(Co), the B band maxima is at 423 nm and the Q (1,0), Q (0,0) peaks are at 535 nm and 568 nm. The decrease in the number of Q bands upon core metalation can be assigned to the increase in molecular symmetry from D_{2h} to D_{4h}. The Soret band ($S_2 \leftarrow S_0$) of PPIX is broader than the two metalated complexes probably due to the dimerization of the free ligands. As metal ion incorporation slightly reduces the possibility of aggregation, the B band became narrower. The structure and the absorption spectra of SQ2 in DMSO (Fig. 1d) show that the highest intensity peak appearing at 664 nm corresponds to the π–π^* transitions while the lower intensity peak at 611 nm is a consequence of dye aggregation. From the absorption spectra of PPIX (Fig. 1a) and SQ2 (Fig. 1d) it is evident that if a mixture of these two sensitizers can be used in an appropriate ratio to sensitize a nanomaterial, the entire visible region of the solar spectrum i.e. 400–700 nm can be harvested. The combination of the absorption spectra of SQ2 with PP(Co) or PP(Zn) also emulates a wide range of solar spectra but the central metal ion of PP is observed to possess a very pronounced effect on the light harvesting efficiency as manifested by the catalysis results explained later.

Depending on the nature of the central metal ion the metalloporphyrins are divided into two groups "Regular" and "Hypso" porphyrins where the first one consists of a closed shell central metal ion (d^{10} or d^0) and the second one consists of a metal ion which has a vacant d orbital (d^n, n = 6–9).[42]

10420 | Phys. Chem. Chem. Phys., 2018, 20, 10418–10429
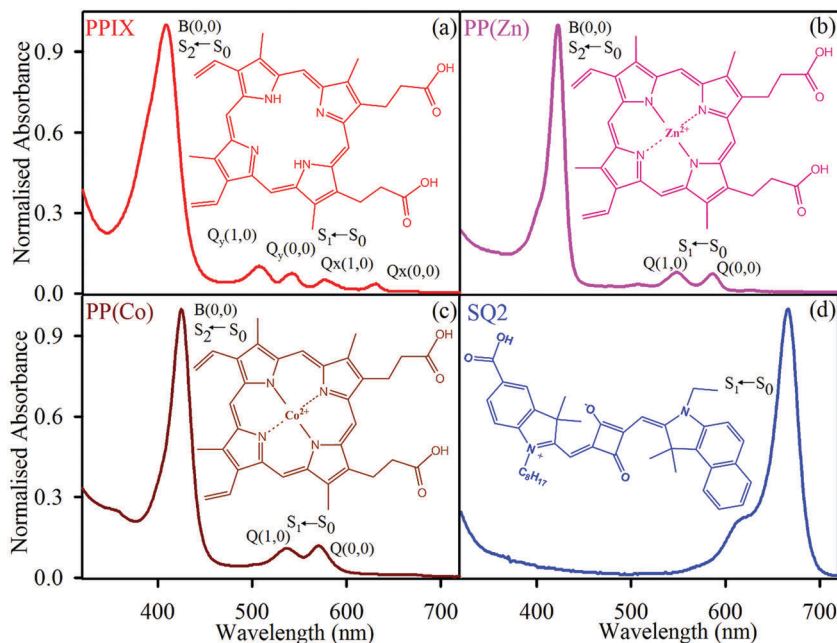
This journal is © the Owner Societies 2018

Fig. 1 Molecular structure and normalised absorption spectra of (a) PPIX, (b) PP(Zn), (c) PP(Co) and (d) SQ2.

PP(Co) is a hypsoporphyrin with a d^7 central metal ion. From the emission spectra of PPIX and PP(Co) shown in Fig. 2a, it can be observed that the fluorescence intensity is drastically reduced upon cobalt(II) ion incorporation in the porphyrin moiety. The intramolecular charge separation from the $a_{2u}(\pi)$ of the ligand porphyrin to the vacant d_{z^2} orbital of the Co(II) metal ion is responsible for the reduction in fluorescence intensity. In hypso-porphyrins, there is a significant overlap between the π^* of porphyrin and the $d\pi$ (d_x and d_y) of the central metal ion which facilitates the metal to ligand back-bonding and as a synergistic effect the $a_{2u}(\pi) \rightarrow d_{z^2}$ charge transfer also becomes facile. From the similar excitation spectra of PPIX and PP(Co) shown in the inset of Fig. 2a, it can be concluded that the very low emission intensity at 630 nm of PP(Co) is attributed to the very small amount of the free PP molecules left in the solution. Fig. 2b shows the steady state emission spectra of PP(Zn) where two prominent emission peaks are observed at 588 nm and 631 nm which are due to Q(0,0) and Q(0,1) transitions, respectively. The emission peak positions are blue shifted in PP(Zn) from that of PPIX due to the reorientation of the electronic levels and this is in good agreement with the absorption spectra of the dyes as discussed earlier. A higher energy gap is associated with PP(Zn) for the increased molecular symmetry rather than PPIX. The intra-molecular charge transfer process is not expected in the case of the regular metaloporphyrin PP(Zn) as Zn(II) is a d^{10} system and it does not have any vacant d orbital to accept the electrons from the protoporphyrin ligand. Additionally, the metal-based $d\pi$ orbitals are low lying in Zn(II), so the possibility of metal to ligand backbonding is also very less in the case of PP(Zn). The excitation spectra of PP(Zn) in the inset of Fig. 2b show two different spectral features for two different emission wavelengths. At 588 nm emission the excitation spectra resemble
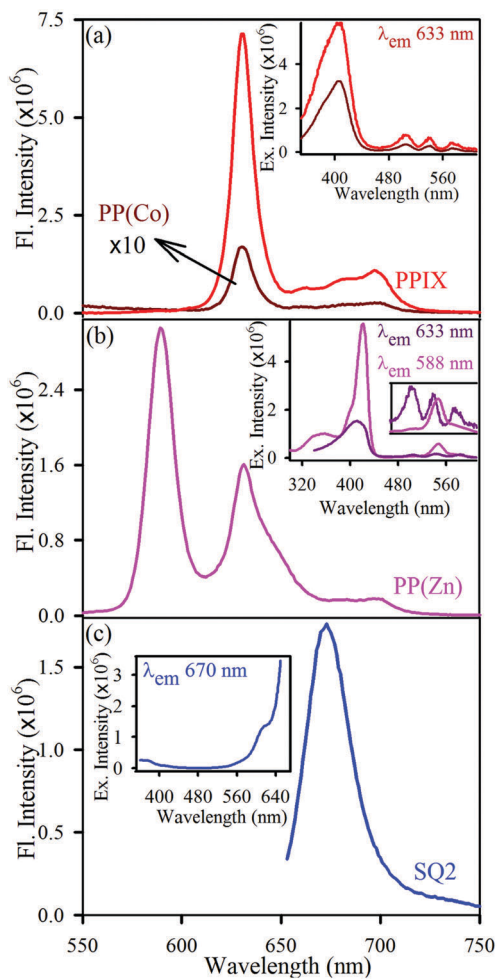

Fig. 2 The steady state fluorescence emission spectra in solvent DMSO for (a) PPIX and PP(Co), (b) PP(Zn) and (c) SQ2. The insets of each show their respective excitation spectra.

This journal is © the Owner Societies 2018

Phys. Chem. Chem. Phys., 2018, **20**, 10418–10429 | **10421**

the absorption spectra of PP(Zn) whereas at 631 nm emission wavelength, the excitation spectra resemble the absorption spectra of PPIX. The emission maxima of the SQ2 are shown in Fig. 2c, at 672 nm and the corresponding excitation spectra resemble the absorption spectra of SQ2 with an additional signature of $S_0 \rightarrow S_2$ transition around at 380 nm.

Fig. 3a shows the absorption spectra of the sensitized nanohybrids along with the absorption spectra of the bare ZnO NP. The retention of the ZnO band gap peak after being sensitized by different sensitizers proves that sensitizers do not affect the stability of the ZnO nanoparticle. The absorption spectra of the ZnO NP shown in Fig. 3a show a band gap of 3.4 eV. The HOMO–LUMO gap of the sensitizers used in this study is well reported in the literature in various theoretical and experimental studies.[43] The redox potentials of PPIX, PP(Zn) and PP(Co) obtained from CV are 0.46 V, 0.57 V, 0.67 V, respectively, with respect to the saturated calomel electrode.[44] On the other hand, the reduction potential of squaraine obtained from CV is −0.78 V with reference to NHE.[45] The TEM image of the ZnO NP shown in Fig. 3b shows an interplanar distance of ~0.26 nm, corresponding to the spacing between two (002) planes. The ZnO NP (~30 nm) used in this study has a zeta potential (mV)/average agglomerate size (nm) of −3.00/1170 at pH 7.4.[46] To obtain the details of attachment of the dyes on the ZnO surface, we analyzed the FTIR spectra of SQ2_ZnO and PP_ZnO conjugates and compared them to that of free SQ2 and PPIX. As shown in Fig. 4, the FTIR peaks corresponding to the carboxylic group stretching frequency of the free dyes were found to disappear and shift respectively for

the two conjugates while the other peaks remained the same. This perturbation in the stretching frequency at 1695 cm^{-1} in the case of PPIX and 1685 cm^{-1} in the case of SQ2 proves their attachment to the ZnO surface through carboxylic groups. The attachment of the carboxylic group of the sensitizer to Zn(II) located at the ZnO surface can further be proved from the Raman spectra of the functionalized nanohybrids as shown in our earlier publication.[23] From thermogravimetric analysis and a particle density of ~30 nm ZnO NP, we have estimated that ~15 000 SQ2 and ~3500 PPIX were attached with one ZnO NP at 8:2 molar ratio of the SQ2:PPIX sensitizers. The estimated value is consistent with earlier reports.[23] Upon attachment to the ZnO NP surface, the steady state emission of the sensitizers is quenched as shown in Fig. 3c and d. In addition, the steady state emission peak of PPIX in the PPIX–ZnO nanohybrid is red-shifted by ~5 nm compared to the emission spectra of free PPIX. This observation indicates the electronic interaction between the singlet excited state of PPIX with the ZnO nanoparticle. The ~6 nm blue shift in the emission peak position of SQ2_ZnO with respect to that of free SQ2 is indicative of a probable aggregation.

To analyze the photoinduced chemical and physical properties of the individual sensitizers and their respective nanohybrids with ZnO, the pico-second resolved fluorescence transients (Fig. 5) were studied. The mechanistic explanation and dynamic behavior of the photo excited charge carriers are co-related with the excited state lifetimes summarized in Table 1. The ZnO NP (~30 nm) has no emission at the excitation wavelengths used in this study (409 nm and 633 nm). Thus, there is no possibility of
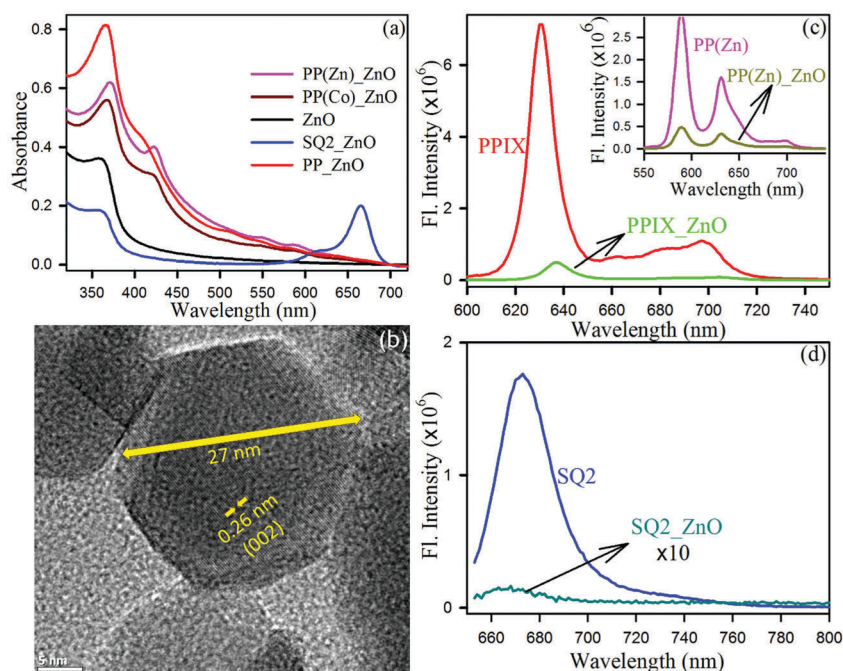
Fig. 3 (a) Absorption spectra of PP(Zn)_ZnO (pink), PP(Co)_ZnO (brown), ZnO NP (black), SQ2_ZnO (blue), PP_ZnO (red), (b) TEM image of a ZnO nanoparticle (c) emission spectra of the PPIX_ZnO compared to PPIX, inset shows the steady state emission spectra of PP(Zn)_ZnO compared to that of PP(Zn), and (d) steady state emission spectra of SQ2_ZnO compared to that of SQ2. The emission spectra of SQ2_ZnO are ten times multiplied to show the changes.

10422 | Phys. Chem. Chem. Phys., 2018, 20, 10418–10429
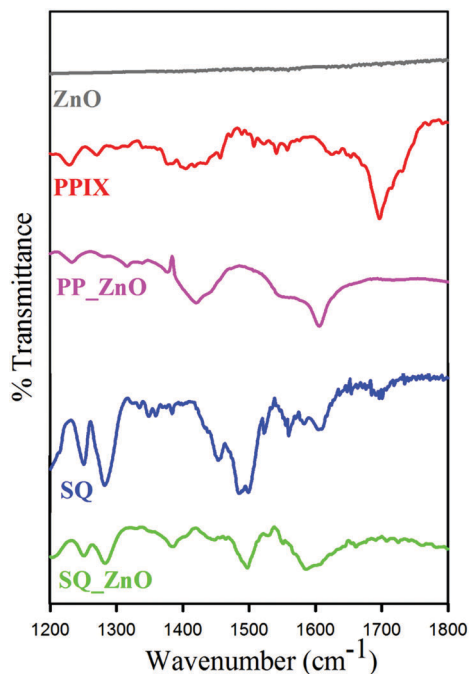
This journal is © the Owner Societies 2018

Fig. 4 FTIR spectra of ZnO NP (grey), PP (red), PP-ZNO (pink), SQ2 (blue) and SQ2_ZnO (green).

interference in the decay patterns of the sensitizers from the ZnO defect state emission. In DMSO solvent, both PPIX and PP(Zn) show single exponential lifetimes of 16.50 ns and 2.24 ns, respectively. Kobayashi *et al.* have reported earlier that the decay lifetime and quantum yield of the S_1 state emission in porphyrin systems decrease with an increase in the atomic number of the central metal ion or the ligand as well due to enhanced spin–orbit coupling and acceleration of intersystem crossing.[47] In the case of fluorescence decay lifetime of PP(Co), a fast component of 240 ps with 38% relative weightage is observed upon excitation at 409 nm because of the ligand to metal charge transfer. Regarding the excited state lifetime of the dye–ZnO complexes, both PPIX and PP(Zn) show efficient ligand to semiconductor electron transfer with timescales in hundreds of picosecond range. A very low extent of ligand to semiconductor charge transfer takes place in the PP(Co)_ZnO complex which is also evident from the reduced average lifetime of the complex compared to the dye PP(Co) but the lifetime of that particular process is not much distinguishable from that of the ligand to metal charge transfer timescale. The fluorescence lifetime of the SQ2 dye is measured to be single exponential while upon attachment to the ZnO surface, an additional 80 ps faster component in lifetime appeared due to the electron transfer from SQ2 to ZnO. As there is no IRF like component in the decay pattern of SQ2_ZnO, there is no possibility of any predominant electron injection in sub-picosecond time scales.[48]

The steady state quenching of donor emission for both PPIX and PP(Zn) after the addition of SQ2 is shown in Fig. 6. As shown in the insets of Fig. 7a and b, there is a significant overlap between the absorption spectra of the NIR absorbing sensitizer SQ2 and the emissions of the visible absorbing sensitizers PPIX and PP(Zn). In order to investigate the possibility of resonance energy transfer between the donor PPIX or PP(Zn) and the acceptor SQ2, time resolved fluorescence decays are measured in a mimic of the proposed ZnO nanohybrid systems by attaching both the donor and the acceptor on the surface of <50 nm Al_2O_3. The aim of attaching the donor and
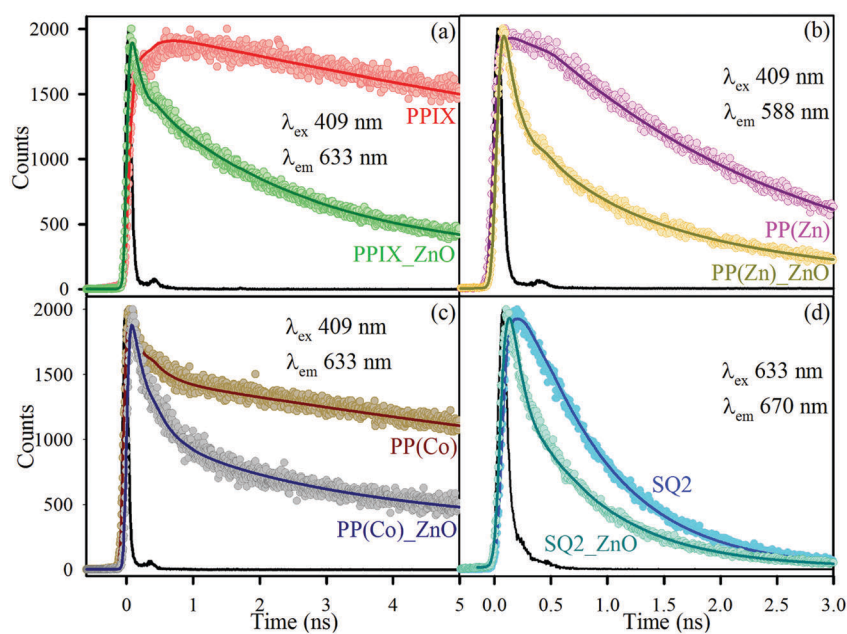

Fig. 5 Pico-second resolved fluorescence decay profiles of (a) PPIX (red) and PPIX attached to ZnO (green), (b) PP(Zn) (pink) and PP(Zn) attached to ZnO (yellow) (c) PP(Co) (brown) and PP(Co) attached to ZnO (grey). (d) SQ2 (blue) and SQ2 attached to ZnO (cyan). All the measurements were performed in DMSO solvent.
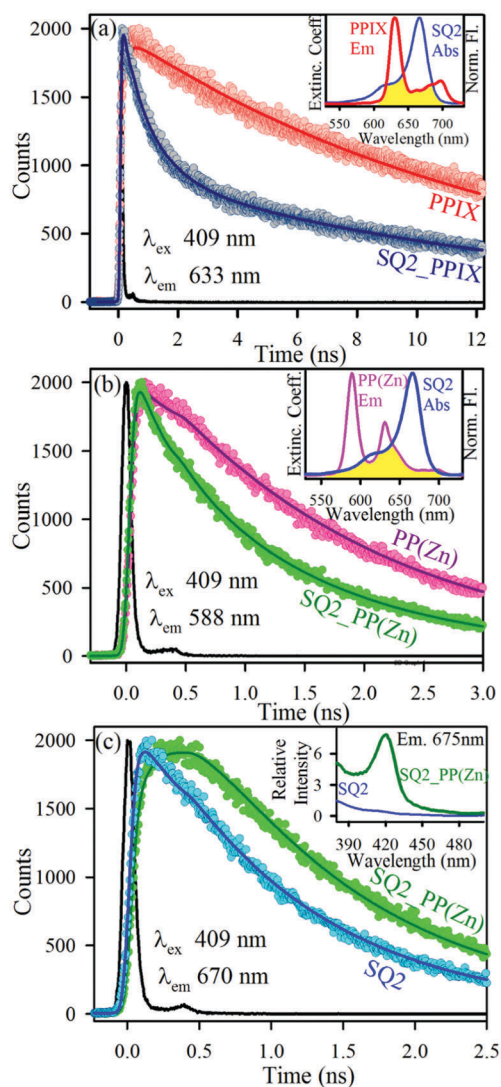
This journal is © the Owner Societies 2018

Phys. Chem. Chem. Phys., 2018, **20**, 10418–10429 | 10423

Table 1 Dynamics of picosecond resolved fluorescence transients of the dyes PPIX, PP(Zn), PP(Co) and SQ2 and the respective nanohybrids with ZnO

Sample	Excitation wavelength (nm)	Emission wavelength (nm)	τ_1 (ns)	τ_2 (ns)	τ_3 (ns)	τ_{avg} (ns)
PPIX	409	633	16.50 ± 0.10 (100%)			16.50
PPIX_ZnO	409	633	16.50 ± 0.10 (13%)	2.25 ± 0.05 (44%)	0.13 ± 0.03 (42%)	3.19
PP(Co)	409	633	16.50 ± 0.10 (62%)	0.24 ± 0.03 (38%)		10.32
PP(Co)_ZnO	409	633	16.50 ± 0.10 (23%)	2.17 ± 0.05 (22%)	0.24 ± 0.03 (55%)	4.40
PP(Zn)	409	588	2.24 ± 0.03 (100%)			2.24
PP(Zn)_ZnO	409	588	2.24 ± 0.03 (25%)	0.59 ± 0.02 (29%)	0.10 ± 0.03 (44%)	0.78
SQ2	633	670	0.73 ± 0.04 (100%)			0.73
SQ2_ZnO	409	670	0.73 ± 0.05 (34%)	0.08 ± 0.02 (66%)		0.30
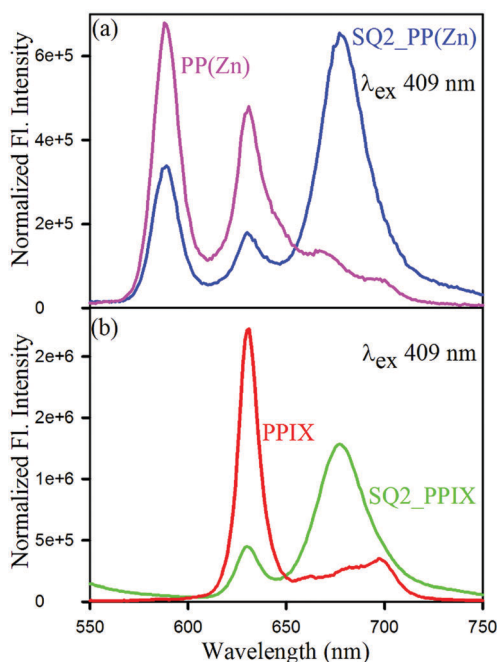
Fig. 6 Steady state Pl spectra of (a) PP(Zn) and SQ2_PP(Zn) attached to Al$_2$O$_3$. (b) PPIX and SQ2_PPIX attached to Al$_2$O$_3$.

Fig. 7 The picosecond resolved fluorescence decay of (a) PPIX attached to Al$_2$O$_3$ in the absence (red) and presence (grey) of SQ2. (b) PP(Zn) attached to Al$_2$O$_3$ in the absence (pink) and presence (green) of SQ2. The inset shows the spectral overlap between the emission of PP(Zn) and absorption of SQ2, (c) time resolved fluorescence decay of SQ2 attached to Al$_2$O$_3$ in the absence (blue) and presence of PP(Zn). The inset shows the excitation spectra of SQ2 in the absence and presence of PP(Zn).

acceptor dyes to Al$_2$O$_3$ for investigation of FRET (Förster resonance energy transfer) is to bring them in enough proximity to each other enabling the possibility of intermolecular dipole–dipole coupling. As Al$_2$O$_3$ is an insulator, insignificant charge transfer possibility upon attachment of the dyes to the nanoparticle surface is evident in the literature.[49] Thus, all the three dyes PPIX, PP(Zn) and SQ2 have a single exponential lifetime even after being attached to the Al$_2$O$_3$ surface.

Fig. 7a shows that the fluorescence of the donor PPIX attached to Al$_2$O$_3$ decays at a single exponential lifetime and after the addition of the acceptor SQ2 the average lifetime is observed to be quenched. A similar trend in the change of lifetime after the addition of the acceptor SQ2 is observed for another donor molecule PP(Zn) also (Fig. 7b). For the donor PP(Zn), we are able to capture the rise in the acceptor's decay profile in a solution mixture of PP(Zn) and SQ2 upon excitation at 409 nm (Fig. 7c) which provides a strong evidence of the FRET between these two dye pairs. In the inset of Fig. 7c, the excitation spectra of only SQ2 and the PP(Zn)–SQ2 FRET pair

are compared at an emission wavelength of 675 nm. It is evident that in the FRET pair the acceptor's emission comes

to some extent from the excitation at the absorption peak position of the donor PP(Zn). Due to resonance energy transfer from the excited state of the donor to that of the acceptor, the decay lifetime of donor has been quenched. Additionally, FRET increases the carrier population in the excited state of the acceptor SQ2 which is responsible for the rise component in the acceptor decay profile upon exciting the donor PP(Zn). So, the average lifetime of the acceptor SQ2 is observed to be increased from 1.10 ns to 2.12 ns after FRET from the donor PP(Zn). Comparing the excited state decay lifetimes of the PP(Zn)–SQ2 system at the emission peak position of PP(Zn) (588 nm) and the emission peak position of SQ2 (670 nm), it can be observed that both of them has the same three lifetime components. Only their relative weightage differs for different emission wavelengths. Both the faster decay lifetime at 588 nm and the rise lifetime at 670 nm are found to be the same. So, the resonance energy transfer between the PP(Zn) and SQ2 is quite evident from all the above-mentioned observations. The rise in the decay profile of SQ2 is not distinguishable in the case of the PPIX–SQ2 pair, as the emission peak of PPIX (633 nm) is very close to the emission peak of the acceptor SQ2 (670 nm), unlike the PP(Zn)–SQ2 pair. All the corresponding timescales and their relative percentage are summarized in Table 2. Using conventional methodologies, the FRET efficiencies between the PPIX–SQ2 pair and the PP(Zn)–SQ2 pair are calculated to be 58% and 44%, respectively. For both the pairs, the overlap integral between the donor emission and acceptor absorption $J(\lambda)$, donor–acceptor distances R_{DA} and other FRET parameters are provided in Table 3. In time resolved measurements, no changes are found in the PP(Co) decay profile upon the addition of SQ2. Thus, it can be concluded that the FRET is absent in the case of the PP(Co) and SQ2 pair due to the other ultrafast competing process of LMCT.

In order to investigate the effect of FRET on the photo-catalytic activity, co-sensitized ZnO nanohybrids are prepared using the dyes PPIX and SQ2 at different molar ratios. Acridine orange (AO) is used as a model organic pollutant to be degraded by the synthesized photocatalysts. Fig. 8a shows the photocatalytic degradation profile of AO under visible light by a co-sensitized photocatalyst. A hypso-chromic shift in the absorption peak of photodegraded AO and discoloration of the solution due to lower molar extinction coefficient of the photo-degraded products prove the photocatalysis of AO in the present study. The kinetics of the photodegradation of AO is shown in the inset of Fig. 8a where the rate constant is found to be 0.04 min^{-1}. Fig. 8b shows the photo-degradation of AO under visible light illumination by the nanohybrids co-sensitized with different molar ratios of the two dyes PPIX and SQ2 along with the single dye sensitized nanohybrids *i.e.* PPIX_ZnO and SQ2_ZnO.
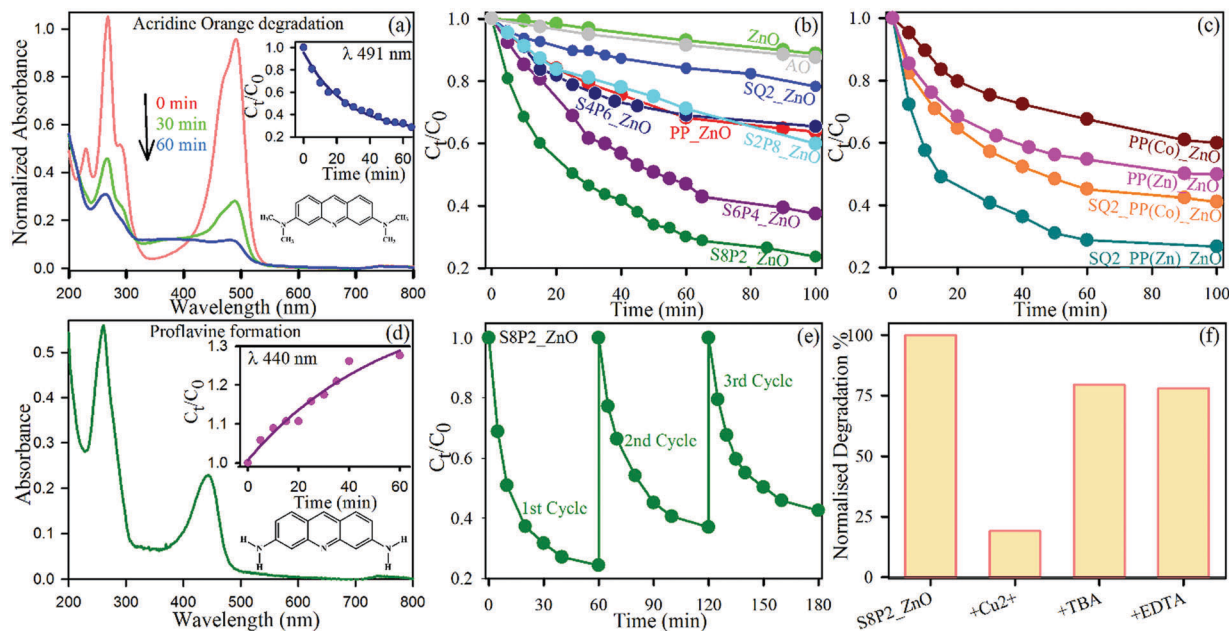
Table 3 FRET parameters

System	$J(\lambda)$	R_0 (nm)	E (%)	R_{DA} (nm)
SQ2_PPIX	1.8×10^{23}	4.5	58	4.2
SQ2_PP(Zn)	1.2×10^{23}	3.2	44	3.3

From the photocatalytic degradation data of AO under visible light (above 395 nm) in 1 h summarized in Table 4, it can be observed that ZnO sensitized by 8 : 2 molar ratio of SQ2 : PPIX shows much better visible light photocatalytic activity than the other molar ratios and the individual dye sensitized nanohybrids. The SQ2_ZnO shows the lowest catalytic activity probably because of the extensive aggregation problem which may have reduced upon co-adsorption with PPIX. Control studies have been done with only AO or only ZnO under visible light illumination but its degradation is negligible. The 8 : 2 molar ratio of SQ2 and PPIX is found to have superior photo catalytic activity among the other molar ratios because at that particular ratio the probability of FRET is the highest which is similar to an earlier observation in the case of co-sensitized DSSCs.[33] To check whether the extent of dipole–dipole coupling can control the catalytic activity, two more co-sensitized nanohybrids are prepared at the same best performing molar ratio of 8 : 2 of the SQ2 and the other visible absorbing metalo-porphyrin dye. These nanohybrids are named SQ2_PP(Co)_ZnO and SQ2_PP(Zn)_ZnO and their catalytic activities are compared to those of the single dye sensitized nanohybrids PP(Co)_ZnO and PP(Zn)_ZnO as shown in Fig. 8c. The figure clearly depicts that both the mixed dye hybrids show better activity than their respective control study of single dye sensitized nanohybrids because in both the cases the absorption window is increased due to co-sensitization. But the notable feature is that SQ2_PP(Zn)_ZnO shows a much higher activity than SQ2_PP(Co)_ZnO as in the latter the dipole–dipole coupling effect is absent. The activity of S8P2_ZnO and SQ2_PP(Zn)_ZnO is found to be similar as in both the cases, FRET is a photo-induced process which facilitates the enhanced radical generation and the pollutant degradation as well. The *N*-De-methylation process occurs during photo degradation of acridine orange (AO). The four *N*-methyl groups are removed from the original AO moiety during photo-degradation.[50] 3,6-Diaminoacridine or proflavine has been widely reported as the photo-degraded product of acridine orange due to ROS mediated photocatalysis. Fig. 8d shows the absorption spectra of proflavine (PF) and the inset of Fig. 8d shows the kinetics of formation of the product proflavine derived from a peak normalized degradation profile of AO. The formation of PF is took place

Table 2 Excited state lifetime of the donor PPIX and PP(Zn) attached to Al$_2$O$_3$ in the presence and absence of the acceptor SQ2 and the excited state lifetime of the acceptor SQ2 attached to Al$_2$O$_3$ in the presence and absence of the donor PP(Zn)

Sample	Excitation wavelength (nm)	Emission wavelength (nm)	τ_1 (ns)	τ_2 (ns)	τ_3 (ns)	τ_{avg} (ns)
PPIX	409	633	13.20 ± 0.10 (100%)			13.20
PPIX–SQ2	409	633	13.20 ± 0.10 (38%)	1.02 ± 0.05 (39%)	0.25 ± 0.01 (23%)	5.47
PP(Zn)	409	588	1.90 ± 0.06 (100%)			1.90
PP(Zn)–SQ2	409	588	1.90 ± 0.05 (26%)	1.10 ± 0.04 (45%)	0.25 ± 0.03 (28%)	1.06
SQ2	409	670	1.10 ± 0.10 (100%)			
PP(Zn)–SQ2	409	670	1.90 ± 0.10 (34%)	1.10 ± 0.04 (152%)	0.25 ± 0.03 (−86%)	2.12

This journal is © the Owner Societies 2018

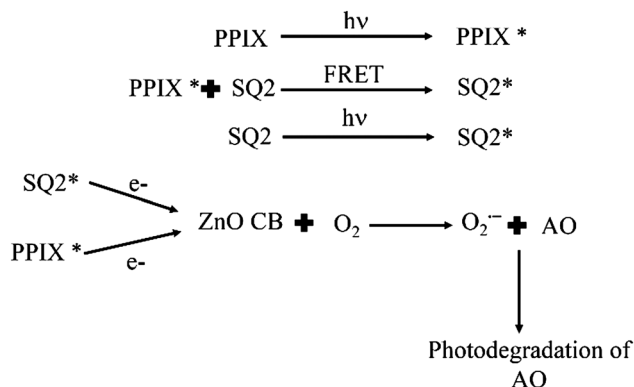*Phys. Chem. Chem. Phys.*, 2018, **20**, 10418–10429 | **10425**

Fig. 8 Photocatalysis under visible light irradiation (above 395 nm) (a) photocatalytic degradation of acridine orange (AO) by the SQ2 and PPIX (8 : 2) co-sensitized ZnO, inset shows the kinetics at the absorption peak maxima of acridine orange, (b) comparison of catalytic activity for different co-sensitized ZnO sensitized by different ratios of SQ2 and PPIX, control ZnO and acridine orange. (c) Catalytic activity of ZnO sensitized by PP(Co), PP(Zn) and by their respective cocktail mixture with SQ2 at 8 : 2 molar ratio of SQ2 and the metalloporphyrins. (d) Absorption spectra of the photo-degraded product proflavine (PF), the inset shows the kinetics at the absorption peak maxima of PF during photocatalysis of AO obtained from a normalized absorption spectra of AO degradation. (e) Recyclability of the catalyst S8P2_ZnO *i.e.* ZnO sensitized by 8 : 2 molar ratio of SQ2 and PPIX. (f) Effects of Cu^{2+}, TBA and EDTA on the photocatalytic activity of S8P2_ZnO.
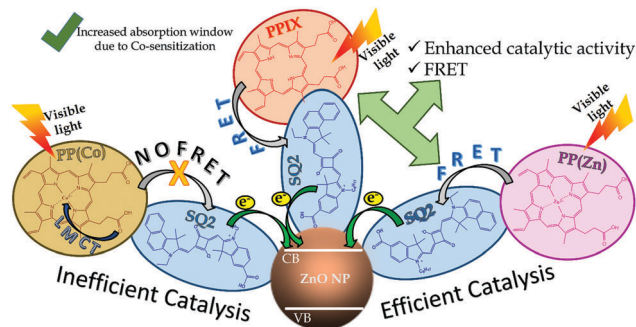
at a rate constant of 0.018 min^{-1} which is slower than the degradation rate of AO due to the formation of several intermediate products. The comparison of the decay kinetics of AO and formation of proflavine further proves the photo-degradation. The recyclability of the co-sensitized nanohybrid S8P2_ZnO has also been tested and Fig. 8e shows that the catalyst is still 50% active after completion of three cycles. After consecutive cycles, the activity decreases probably due to the dye leaching process.

To explore the mechanism of catalytic activity of the SQ2 and PPIX co-sensitized nanohybrid, catalysis has been performed in the presence of excess radical scavengers and the results are shown in Fig. 8f. Cu^{2+} is known as an electron scavenger because it accepts electrons from the reaction media to yield Cu^+. Tertiary butyl alcohol (TBA) acts as the scavenger of $^\bullet OH$, and ethylene-diaminetetraacetic acid (EDTA) is introduced as a hole (h^+) quencher. In all the three cases the catalytic activity decreases but Cu^{2+} has reduced the activity drastically to 20% which implies that among all the reactive species the negatively charged $O_2^{\bullet-}$ plays the most crucial role in the photo-degradation of the pollutant. Comparing all the catalytic activities tabulated in Table 4, it can be inferred that in the case of co-sensitized photocatalyst synthesis, FRET is a dynamic event which has much pronounced influence in controlling the light harvesting activity, and the nature of the specific metal ion in the porphyrin core plays a crucial role in the dipole–dipole coupling with the acceptor dye. The predominant mechanistic pathway under visible light catalysis of the nanohybrids is summarized in the following chemical equations and Scheme 1.

Table 4 Percentage of photocatalytic degradation of acridine orange in the presence of different catalysts in 1 h

Catalyst	Photocatalytic degradation (%) of AO in 1 h
PP_ZnO	32 ± 2
SQ2_ZnO	16 ± 1
SQ2 : PP (8 : 2)_ZnO	70 ± 3
SQ2 : PP (6 : 4)_ZnO	54 ± 2
SQ2 : PP (4 : 6)_ZnO	31 ± 2
SQ2 : PP (2 : 8)_ZnO	29 ± 2
ZnO	8 ± 1
AO	9 ± 1
SQ2 : PP(Co) (8 : 2)_ZnO	55 ± 2
SQ2 : PP(Zn) (8 : 2)_ZnO	72 ± 3
PP(Co)_ZnO	33 ± 2
PP(Zn)_ZnO	46 ± 2

$$PPIX \xrightarrow{h\nu} PPIX^*$$

$$PPIX^* + SQ2 \xrightarrow{FRET} SQ2^*$$

$$SQ2 \xrightarrow{h\nu} SQ2^*$$

$$SQ2^* \xrightarrow{e^-} ZnO\ CB + O_2 \longrightarrow O_2^{\bullet-} + AO$$
$$PPIX^* \xrightarrow{e^-}$$

$$\downarrow$$

$$\text{Photodegradation of AO}$$

Scheme 1 FRET: the tuning tool for modulating the catalytic activity of co-sensitized nanohybrids, under visible light illumination.

Table 5 Percentage of photocatalytic degradation of acridine orange in the presence of different catalysts in 1 h under NIR light irradiation (above 650 nm) using a tungsten–halogen light source

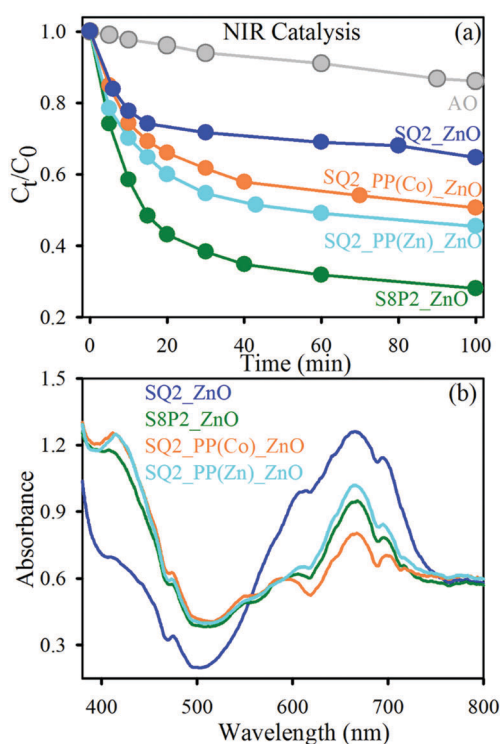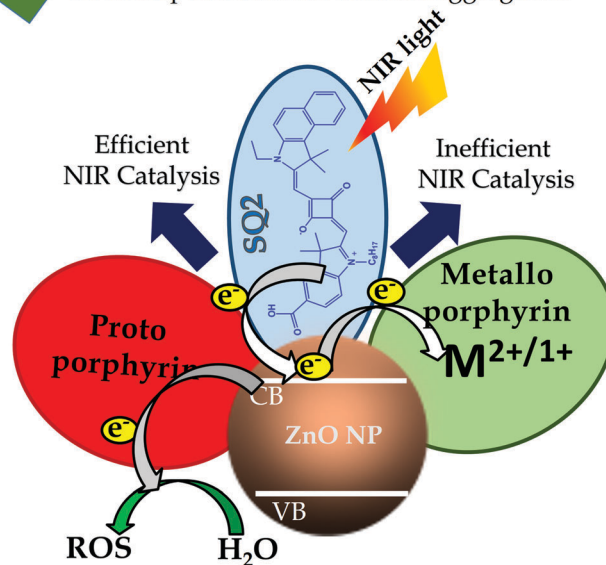| Catalyst	Photocatalytic degradation (%) of AO in 1 h
AO	9 ± 1
SQ2_ZnO	31 ± 2
SQ2 : PP (8 : 2)_ZnO	69 ± 2
SQ2 : PP(Co) (8 : 2)_ZnO	45 ± 1
SQ2 : PP(Zn) (8 : 2)_ZnO	51 ± 2

Fig. 9 (a) Photocatalytic activities under NIR light irradiation (above 650 nm) using a tungsten–halogen light source, (b) dye loading in different nanohybrids from solid state absorption spectra collected in retro reflecting mode.

Scheme 2 Photocatalysis under NIR light illumination by three co-sensitized nanohybrids.

Fig. 9a shows NIR light induced photocatalysis by the co-sensitized nanohybrids. From the comparison of the dye degradation percentages summarized in Table 5, it is quite evident that the co-sensitized nanohybrids exhibit better catalytic activity under NIR light than the control SQ2–ZnO. However, the dye loading curve in Fig. 9b shows that there is higher loading of SQ2 in the SQ2–ZnO hybrid rather than the other co-sensitized hybrids. This observation leads to the conclusion that higher loading causes a stronger aggregation which is clear from the monomer–dimer peak ratio of the SQ2–ZnO and the three co-sensitized photocatalysts. In the co-sensitized nanohybrids, aggregation is suppressed to some extent due to co-adsorption on the ZnO surface. The SQ2_PPIX_ZnO adduct is found to exhibit the best NIR catalysis with 69% dye degradation

in 1 h while SQ2_PP(Zn)_ZnO and SQ2_PP(Co)_ZnO show comparatively less activities due to the presence of the metal centre. The phenomenon is well explained in Scheme 2. The excited state electrons of SQ2 are trapped in the porphyrin core-metal through the ZnO conduction band. It has been reported earlier that photoexcited carriers of the semiconductor conduction band move to the core metal of the metalloporphyrin photosensitizers[51,52] and facilitate charge separation under UV irradiation but in the case of dual dye sensitization the same phenomenon is observed to diminish the NIR catalytic activity of the conjugate. As cobalt has a vacant d orbital, the process is more facile in the case of PP(Co) than PP(Zn). Thus, SQ2_PP(Co)_ZnO performs less efficiently than SQ2_PP(Zn)_ZnO. It can be inferred that for NIR catalysis PPIX is proved to be a better co-adsorbent for SQ2–ZnO than the other two metalloporphyrins.

4. Conclusion

Our present study on PPIX, PP(Co), PP(Zn) and SQ2 dyes provides an insight into their excited state dynamic behavior

This journal is © the Owner Societies 2018

Phys. Chem. Chem. Phys., 2018, **20**, 10418–10429 | 10427

for their potential use as light harvesting photo-sensitizers. We have shown that the dipolar coupling or FRET from PPIX to SQ2 at the ZnO surface plays the key role to enhance the catalytic activity of the co-sensitized photocatalyst. Most importantly, the dipole–dipole coupling of the PPIX and SQ2 pair is observed to be highly influenced by the core metalation of the donor PPIX and consequently affecting the catalytic activity of the co-sensitized ZnO nanohybrid under visible light. In the case of PP(Co) the FRET is found to be absent due to ultrafast photo-induced ligand to metal charge transfer. At the same time PP(Zn)–SQ2 is observed to be a very efficient FRET pair. Photo-catalytic efficiency is also conclusively correlated with the presence and absence of FRET. Additionally, the PPIX–SQ2 co-sensitized ZnO nanohybrid is observed to be an efficient NIR photocatalyst also due to the anti-aggregation effect of PPIX on the SQ2 molecule at the surface of ZnO. Thus, different ultrafast phenomena have been proved to be the tuning tool for the visible light harvesting as well as NIR harvesting capacity of co-sensitized nanohybrids.

Conflicts of interest

There are no conflicts to declare.

Acknowledgements

References

1 X. Guo, W. Song, C. Chen, W. Di and W. Qin, *Phys. Chem. Chem. Phys.*, 2013, **15**, 14681–14688.

2 J. Chen, S. Shen, P. Guo, M. Wang, J. Su, D. Zhao and L. Guo, *J. Mater. Res.*, 2014, **29**, 64–70.

3 S. Rajaambal, K. Sivaranjani and C. S. Gopinath, *J. Chem. Sci.*, 2015, **127**, 33–47.

4 Q. Daniel, R. B. Ambre, B. Zhang, B. Philippe, H. Chen, F. Li, K. Fan, S. Ahmadi, H. K. Rensmo and L. Sun, *ACS Catal.*, 2017, **7**, 1143–1149.

5 T. Bora, K. K. Lakshman, S. Sarkar, A. Makhal, S. Sardar, S. K. Pal and J. Dutta, *Beilstein J. Nanotechnol.*, 2013, **4**, 714.

6 S. Sardar, P. Kar, H. Remita, B. Liu, P. Lemmens, S. K. Pal and S. Ghosh, *Sci. Rep.*, 2015, **5**, 17313.

7 S. Chu and A. Majumdar, *Nature*, 2012, **488**, 294.

8 X. Chen, C. Li, M. Grätzel, R. Kostecki and S. S. Mao, *Chem. Soc. Rev.*, 2012, **41**, 7909–7937.

9 E. Kowalska, K. Yoshiiri, Z. Wei, S. Zheng, E. Kastl, H. Remita, B. Ohtani and S. Rau, *Appl. Catal., B*, 2015, **178**, 133–143.

10 M. D. Hernández-Alonso, F. Fresno, S. Suárez and J. M. Coronado, *Energy Environ. Sci.*, 2009, **2**, 1231–1257.

11 D. Pei and J. Luan, *Int. J. Photoenergy*, 2011, **2012**, 262831.

12 M. J. Griffith, K. Sunahara, P. Wagner, K. Wagner, G. G. Wallace, D. L. Officer, A. Furube, R. Katoh, S. Mori and A. J. Mozer, *Chem. Commun.*, 2012, **48**, 4145–4162.

13 L. M. Gonçalves, V. de Zea Bermudez, H. A. Ribeiro and A. M. Mendes, *Energy Environ. Sci.*, 2008, **1**, 655–667.

14 R. Y.-Y. Lin, Y.-S. Yen, Y.-T. Cheng, C.-P. Lee, Y.-C. Hsu, H.-H. Chou, C.-Y. Hsu, Y.-C. Chen, J. T. Lin and K.-C. Ho, *Org. Lett.*, 2012, **14**, 3612–3615.

15 E. Stathatos, *Solar cells dye-sensitized devices*, InTech, Rijeka, Croatia, 2011, pp. 471–491.

16 J. Chang, C.-P. Lee, D. Kumar, P.-W. Chen, L.-Y. Lin, K. J. Thomas and K.-C. Ho, *J. Power Sources*, 2013, **240**, 779–785.

17 L.-Y. Lin, M.-H. Yeh, C.-P. Lee, J. Chang, A. Baheti, R. Vittal, K. J. Thomas and K.-C. Ho, *J. Power Sources*, 2014, **247**, 906–914.

18 X. Zhang, T. Peng, L. Yu, R. Li, Q. Li and Z. Li, *ACS Catal.*, 2014, **5**, 504–510.

19 Z. Li, Y. Wu and G. Lu, *Appl. Catal., B*, 2016, **188**, 56–64.

20 Z. Xue, L. Wang and B. Liu, *Nanoscale*, 2013, **5**, 2269–2273.

21 P. J. Holliman, M. L. Davies, A. Connell, B. V. Velasco and T. M. Watson, *Chem. Commun.*, 2010, **46**, 7256–7258.

22 B. E. Hardin, A. Sellinger, T. Moehl, R. Humphry-Baker, J.-E. Moser, P. Wang, S. M. Zakeeruddin, M. Grätzel and M. D. McGehee, *J. Am. Chem. Soc.*, 2011, **133**, 10662–10667.

23 S. Sardar, S. Chaudhuri, P. Kar, S. Sarkar, P. Lemmens and S. K. Pal, *Phys. Chem. Chem. Phys.*, 2015, **17**, 166–177.

24 H. Choi, I. Raabe, D. Kim, F. Teocoli, C. Kim, K. Song, J. H. Yum, J. Ko, M. K. Nazeeruddin and M. Grätzel, *Chem. – Eur. J.*, 2010, **16**, 1193–1201.

25 Y. Shi, R. Hill, J. H. Yum, A. Dualeh, S. Barlow, M. Grätzel, S. R. Marder and M. K. Nazeeruddin, *Angew. Chem., Int. Ed.*, 2011, **123**, 6749–6751.

26 S. Ito, H. Miura, S. Uchida, M. Takata, K. Sumioka, P. Liska, P. Comte, P. Péchy and M. Grätzel, *Chem. Commun.*, 2008, 5194–5196.

27 H. Choi, S. O. Kang, J. Ko, G. Gao, H. S. Kang, M. S. Kang, M. K. Nazeeruddin and M. Grätzel, *Angew. Chem., Int. Ed.*, 2009, **121**, 6052–6055.

28 P. Ruankham, L. Macaraig, T. Sagawa, H. Nakazumi and S. Yoshikawa, *J. Phys. Chem. C*, 2011, **115**, 23809–23816.

29 G. De Miguel, M. Marchena, B. Cohen, S. Pandey, S. Hayase and A. Douhal, *J. Phys. Chem. C*, 2012, **116**, 22157–22168.

30 Y. Fang, Z. Li, B. Yang, S. Xu, X. Hu, Q. Liu, D. Han and D. Lu, *J. Phys. Chem. C*, 2014, **118**, 16113–16125.

31 S. Das, T. L. Thanulingam, K. G. Thomas, P. V. Kamat and M. George, *J. Phys. Chem.*, 1993, **97**, 13620–13624.

32 S. Das, K. G. Thomas, K. Thomas, V. Madhavan, D. Liu, P. V. Kamat and M. George, *J. Phys. Chem.*, 1996, **100**, 17310–17315.

33 J. Patwari, S. Sardar, B. Liu, P. Lemmens and S. K. Pal, *Beilstein J. Nanotechnol.*, 2017, **8**, 1705–1713.

34 H. Yu, J. Baskin, B. Steiger, C. Wan, F. Anson and A. Zewail, *Chem. Phys. Lett.*, 1998, **293**, 1–8.

10428 | *Phys. Chem. Chem. Phys.*, 2018, **20**, 10418–10429

This journal is © the Owner Societies 2018

35 H.-Z. Yu, J. S. Baskin and A. H. Zewail, *J. Phys. Chem. A*, 2002, **106**, 9845–9854.

36 P. Kar, S. Sardar, E. Alarousu, J. Sun, Z. S. Seddigi, S. A. Ahmed, E. Y. Danish, O. F. Mohammed and S. K. Pal, *Chem. – Eur. J.*, 2014, **20**, 10475–10483.

37 M. Liong, J. Lu, M. Kovochich, T. Xia, S. G. Ruehm, A. E. Nel, F. Tamanoi and J. I. Zink, *ACS Nano*, 2008, **2**, 889–896.

38 T. Bora, H. H. Kyaw, S. Sarkar, S. K. Pal and J. Dutta, *Beilstein J. Nanotechnol.*, 2011, **2**, 681.

39 J. Lakowicz, *Principles of fluorescence spectroscopy*, Kluwer Academic/Plenum Publishers, New York, 1999.

40 S. Sarkar, A. Makhal, T. Bora, S. Baruah, J. Dutta and S. K. Pal, *Phys. Chem. Chem. Phys.*, 2011, **13**, 12488–12496.

41 T. Geiger, S. Kuster, J. H. Yum, S. J. Moon, M. K. Nazeeruddin, M. Grätzel and F. Nüesch, *Adv. Funct. Mater.*, 2009, **19**, 2720–2727.

42 M. Prushan, 2005.

43 S. P. de Visser and M. J. Stillman, *Int. J. Mol. Sci.*, 2016, **17**, 519.

44 V. Narayanan and P. Natarajan, *J. Polym. Sci., Part A: Polym. Chem.*, 1992, **30**, 2475–2488.

45 J.-H. Yum, P. Walter, S. Huber, D. Rentsch, T. Geiger, F. Nüesch, F. De Angelis, M. Grätzel and M. K. Nazeeruddin, *J. Am. Chem. Soc.*, 2007, **129**, 10320–10321.

46 J. M. Berg, A. Romoser, N. Banerjee, R. Zebda and C. M. Sayes, *Nanotoxicology*, 2009, **3**, 276–283.

47 O. Ohno, Y. Kaizu and H. Kobayashi, *J. Chem. Phys.*, 1985, **82**, 1779–1787.

48 J. Kallioinen, G. Benkö, V. Sundström, J. E. Korppi-Tommola and A. P. Yartsev, *J. Phys. Chem. B*, 2002, **106**, 4396–4404.

49 C. Karunakaran, J. Jayabharathi, R. Sathishkumar and K. Jayamoorthy, *Measurement*, 2013, **46**, 3261–3267.

50 C.-S. Lu, C.-C. Chen, L.-K. Huang, P.-A. Tsai and H.-F. Lai, *Catalysts*, 2013, **3**, 501–516.

51 C. Wang, J. Li, G. Mele, G.-M. Yang, F.-X. Zhang, L. Palmisano and G. Vasapollo, *Appl. Catal., B*, 2007, **76**, 218–226.

52 H. Huang, X. Gu, J. Zhou, K. Ji, H. Liu and Y. Feng, *Catal. Commun.*, 2009, **11**, 58–61.

This journal is © the Owner Societies 2018

Phys. Chem. Chem. Phys., 2018, **20**, 10418–10429 | **10429**